Novel Square Arrangements in Tetranuclear and Octanuclear Iron(III) Complexes with Asymmetric Iron Environments Created by the Unsymmetric Bridging Ligand *N*,*N*,*N*′-Tris((*N*-methyl)-2-benzimidazolylmethyl)-*N*′-methyl-1,3-diamino-2-propanol

Joe H. Satcher, Jr.,*,†,§ Marilyn M. Olmstead,*,§ Michael W. Droege,†,‡ Sean R. Parkin,†,§ Bruce C. Noll,§ Leopold May,¥ and Alan L. Balch*,§

Lawrence Livermore National Laboratory, Livermore, California 94550, and Departments of Chemistry, University of California Davis, Davis California, 95616, and The Catholic University of America, Washington, D.C. 20064

Received March 5, 1998

The synthesis and characterization of novel tetranuclear and octanuclear iron(III) complexes with structures based on a nearly square arrangement of four iron ions are reported. Reaction of ferric nitrate, sodium acetate, and the unsymmetrical binucleating ligand HBMDP, where HBMDP is *N*,*N*,*N*′-tris((*N*-methyl)-2-benzimidazolylmethyl)-*N*′-methyl-1,3-diamino-2-propanol, in acetone/water yields the tetranuclear iron complex $[Fe_4(\mu\text{-}O)_2(\mu\text{-}BMDP)_2(\mu\text{-}OAc)_2]^{4+}$, which exhibits coordination number asymmetry. The structure of $[Fe_4(\mu\text{-}O)_2(\mu\text{-}BMDP)_2(\mu\text{-}OAc)_2](NO_3)_3(OH)\cdot 12H_2O$ has been determined by single-crystal X-ray diffraction. Each (μ-BMDP) ligand spans two iron(III) ions and causes these ions to become structurally distinct. Within this binuclear unit one iron atom is five-coordinate with distorted square pyramidal geometry and an N_2O_3 donor set, while the other iron is six-coordinate with distorted octahedral geometry and an N_3O_3 donor set. Two of these binuclear units are linked through a pair of oxo and acetato bridges to form the centrosymmetric tetranuclear complex. The coordinatively nonequivalent iron atoms exhibit distinct Mössbauer spectroscopic parameters and produce a pair of doublets at 80 K. The iron(III) centers are coupled antiferromagnetically with a room-temperature moment of 1.9 μ_B per iron with $J = -103.3$ cm^{-1}, $zJ' = -105.9$ cm^{-1}. The properties of the unsymmetric cation $[Fe_4(\mu\text{-}O)_2(\mu\text{-}BMDP)_2(\mu\text{-}OAc)_2]^{4+}$ are similar to those observed for binuclear iron proteins with comparable coordinative inequivalence. Efforts to increase the solubility of $[Fe_4(\mu\text{-}O)_2(\mu\text{-}BMDP)_2(\mu\text{-}OAc)_2]^{4+}$ by metathesis with sodium tetrafluoroborate resulted in the isolation of crystals of a new octanuclear iron species, $[Fe_8(\mu\text{-}O)_4(\mu\text{-}BMDP)_4(OH)_4(\mu\text{-}OAc)_4](BF_4)_3(OH)\cdot 2CH_3CN\cdot 8H_2O$ (**2**), which has also been characterized by single-crystal X-ray diffraction. The asymmetric unit consists of an $Fe_2(\mu\text{-}O)(\mu\text{-}BMDP)(\mu\text{-}OAc)(OH)$ group which is externally bridged via the oxo ions to form a molecular square with four of the eight iron ions at the corners. Both iron sites are six-coordinate with distorted octahedral geometry. One has an N_2O_4 donor set; the other has an N_3O_3 donor set.

Introduction

A number of polyfunctional ligands have been created to facilitate the construction of binuclear metal complexes as models for the active sites of metalloproteins.[1−3] As a result a host of models for binuclear iron and copper sites as well as polynuclear iron and manganese sites have been developed. Binuclear iron units are found in the active sites of a number of metalloproteins including hemerythrin, ribonucleotide reductase, purple acid phosphatase, and methane monooxygenase.[4−7] Within these binuclear units, the protein environment can facilitate the positioning of the iron sites into distinctly different environments. These environments may differ in their coordination numbers, ligation sets, and coordination geometries. In particular, coordination number asymmetry has been shown to exist in a number of metalloproteins and may impart unique reactivity.[8] Hemerythrin, the prototypical binuclear iron protein, was the first of this group to be characterized by X-ray crystallography.[4c,5] In deoxyhemerythrin, five imidazole groups

* To whom correspondence should be addressed.
† Lawrence Livermore National Laboratory.
‡ Current address: Ocellus Inc., 887A Industrial Rd., San Carlos, CA 94070.
§ University of California, Davis.
¥ The Catholic University of America.

(1) Fenton, D. E.; Okawa, H. *Chem. Ber. Rec.* **1997**, *130*, 433.
(2) Collinson, S. R.; Fenton, D. E. *Coord. Chem. Rev.* **1996**, *148*, 19.
(3) Kitajima, N.; Moro-oka, Y. *Chem. Rev.* **1994**, *94*, 737.
(4) Reviews: (a) Que, L., Jr.; Scarrow, R. C. In *Metal Clusters in Proteins*; Que, L., Jr., Ed.; ACS Symposium Series No. 372; American Chemical Society: Washington, DC, 1988; pp 152−178. (b) Vincent, J. B.; Oliver-Lilley, G. L.; Averill, B. A. *Chem. Rev.* **1990**, *90*, 1447−1467. (c) Stenkamp, R. E. *Chem. Rev.* **1994**, *94*, 715−726. (d) Fraústo da Silva, J. J. R.; Williams, R. J. P. In *Biological Chemistry of the Elements*; Clarendon Press: Oxford, 1991; Chapter 12. (e) Wilkins, P. C.; Wilkins, R. G. *Coord. Chem. Rev.* **1987**, *79*, 195 (f) Que, L., Jr.; True, A. E. *Prog. Inorg. Chem.* **1990**, *38*, 97. (g) Feig, A. L.; Lippard, S. J. *Chem. Rev.* **1994**, *94*, 759. (h) Wilkins, R. G. *Chem. Soc. Rev.* **1992**, *21*, 171−178. (i) Sanders-Loehr, J. In *Iron Carriers and Iron Proteins*; Loehr, T. M., Ed.; VCH: New York, 1989; Vol. 5, pp 373−466. (j) Nordlund, P.; Eklund, H. *J. Mol. Biol.* **1993**, *232*, 123−164. (k) Wallar, B. J.; Lipscomb J. D. *Chem. Rev.* **1996**, *96*, 2625−2657.
(5) (a) Stenkamp, R. E.; Sieker, L. C.; Jensen, L. H. *Proc. Natl. Acad. Sci. U.S.A* **1976**, *73*, 349. (b) Stenkamp, R. E.; Sieker, L. C.; Jensen, L. H.; McCallum, J. D.; Sanders-Loehr, J. *Proc. Natl. Acad. Sci. U.S.A.* **1985**, *82*, 713.
(6) Nordlund, P.; Sjorberg, B.-M.; Eklund, H. *Nature* **1990**, *345*, 593.
(7) (a) Rosenzweig, A. C.; Frederick, C. A.; Lippard, S. J.; Nordlund, P. *Nature* **1993**, *366*, 537. (b) Rosenzweig, A. C.; Nordlund, P.; Takahara, P. M.; Frederick, C. A.; Lippard, S. J. *Chem. Biol.* **1995**, *2*, 409. (c) Elango, N.; Radhakrishman, R.; Froland, W. A.; Wallar, B. J.; Earhart, C. A.; Lipscomb, J. D.; Ohlendorf, D. H. *Protein Sci.* **1997**, *6*, 556.

10.1021/ic9802404 CCC: $15.00
Published on Web 12/28/1998

from histidine residues are unsymmetrically bound to a (μ-hydroxo)bis(μ-carboxylato)diiron(II) core. This arrangement leaves an open coordination site that is available for dioxygen ligation. Dioxygen binding, coupled with electron transfer and proton migration from the hydroxo bridge, results in the formation of an end-bound hydroperoxide ligand that is stabilized by internal hydrogen bonding at the formerly vacant site. For methane monooxygenase, the X-ray crystal structure of the oxidized form contains a semibridging glutamate residue, suggesting coordination number asymmetry for the two metals.[4g,7a] Mössbauer spectroscopy of the reduced state has also produced evidence of different coordination numbers about the two iron centers.[9]

Although coordination asymmetry has been definitively established in some proteins and inferred in others, far fewer studies of synthetic model complexes that exhibit asymmetric coordination have been reported.[1] The deliberate preparation of ligands that present an inherently unsymmetrical ligation environment provides access to the synthesis of new unsymmetrical binuclear model complexes whose structures, spectroscopic features, and reactivities may be compared with polynuclear metalloproteins.

In the present approach, the unsymmetrical ligand (HBMDP) has been synthesized and utilized to investigate the effect of

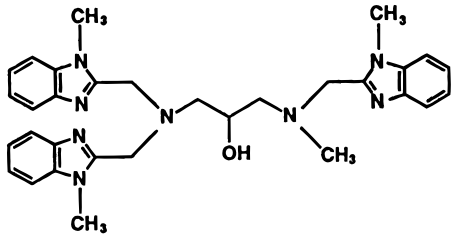

HBMDP

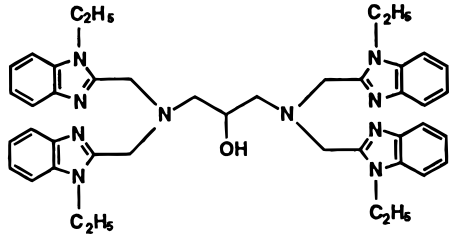

HTBDP

unsymmetrical ligation on binuclear and polynuclear complexes.[10a] HBMDP is related to the symmetrical ligand, HTBDP, that was synthesized earlier by Reed and co-workers to provide models for hemocyanin.[10b] Recently the synthesis, characterization, and chemical reactivity of binuclear copper(II) complexes of HBMDP were reported.[11] That work produced [Cu_2(μ-BMPD)(μ-OAc)](ClO_4)$_2$, which shows coordination number asymmetry with one four-coordinate copper(II) ion and one five-coordinate copper(II) ion.[11] HBMDP also forms an iron complex, [Fe_2(μ-BMPD)(μ-OBz)(MeOH)$_{1.5}$(H_2O)$_{0.5}$](BF_4)$_2$, that displays coordination number asymmetry with one five-coordinate iron(II) ion and one six-coordinate iron(II) ion.[12] Both of these complexes exhibit site-directed reactivity in which ligands add preferentially to the lower coordinate metal ions within each binuclear complex. Thus, the addition of an anionic ligand such as azide or thiocyanate to a solution of either the copper or the iron complex results in binding of the added anion to the four-coordinate copper site or the five-coordinate iron site within the respective complexes. A recent review by Fenton and Okawa on the use of unsymmetrical ligands acknowledges a scarcity of relevant models to mimic coordination asymmetry in polynuclear sites.[1] Only one diiron(III) complex with unsymmetric coordination has been prepared through the use of an unsymmetrical, dinucleating ligand. The product, [Fe_2(μ-MTBPO)(μ-O_2AsMe_2)(MeOH)Cl_2](ClO_4)$_2$, which was obtained through the use of the related unsymmetrical ligand (HMTBPO), has two six-coordinate iron(III) sites: one with an N_2O_3Cl donor set, the other with an N_3O_2Cl donor set.[13]

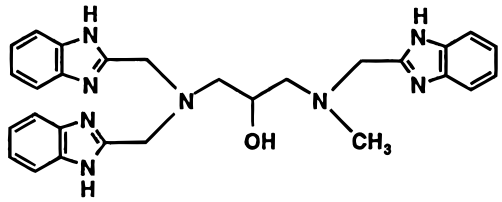

HMTBPO

Results

Synthetic Studies. Iron(III) salts react rapidly with HBMDP in mixtures of aqueous and organic solvents. In this work, ferric nitrate nonahydrate was dissolved in water and added to HBMDP in acetone in a fixed 2:1 ratio. Sodium acetate in water was added in amounts that varied from 0 to 8 equiv per mole of HBMDP. For sodium acetate additions of 0, 1, and 2 equiv, the products that precipitated were either polycrystalline or amorphous. Elemental analysis suggested that complicated mixtures of compounds were present. With the addition of 3 equiv of sodium acetate, a homogeneous, crystalline product, [Fe_4(μ-O)$_2$(μ-BMDP)$_2$(μ-OAc)$_2$](NO_3)$_3$(OH)·$6H_2O$ ([**1**](NO_3)$_3$(OH)·$6H_2O$), was formed in ~19% yield. With increasing amounts of sodium acetate, the yields of the same isolated product increased to a maximum of ~65% at 8 equiv. Although elemental analyses were uniformly consistent with the formulation of [**1**](NO_3)$_3$(OH)·$6H_2O$ for the vacuum-dried material, the crystals formed with greater than 3 equiv of sodium acetate were too small for an X-ray structure determination. The use of other carboxylate ions such as formate, propionate, and benzoate did not yield crystalline materials at any concentration under similar conditions. Alternative syntheses employing various solvents (e.g., methanol, acetonitrile, dichloromethane) and counterions

(8) (a) Fee, J. A. In *Metal Ions in Biological Systems*; Sigel, H., Ed.; Dekker: New York, 1981; Vol. 13, p 259. (b) Kurtz, D. M., Jr. *Chem. Rev.* **1990**, *90*, 585. (c) Deng, H.; Hoffmann, R. *Angew. Chem., Int. Ed. Engl.* **1993**, *32*, 1062.

(9) Fox, B. G.; Hendrich, M. P.; Surerus, K. K.; Andersson, K. K.; Lipscomb. J. D. *J. Am. Chem. Soc.* **1993**, *115*, 3688.

(10) (a) Abbreviations used: HBMDP = *N,N,N*′-tris((*N*-methyl)-2-benzoimidazolylmethyl)-*N*′-methyl-1,3-diamino-2-propanol; OAc = acetate; OBz = benzoate; hdp = *N*-(*o*-hydroxybenzyl)-*N,N*-bis(2-pyridylmethyl)amine; tpa = tris(2-pyridylmethyl)amine; BPh_4 = tetraphenylborate; HTBDP = *N,N,N*′,*N*′-tetrakis((*N*-ethyl)-2-benzoimidazolylmethyl)-1,3-diamino-2-propanol; HPTA = *N,N,N*′,*N*′-1,3-diamino-2-propanoltetraacetate; HMTBPO = *N,N,N*′-tris(2-benzoimidazolylmethyl)-*N*′-methyl-1,3-diamino-2-propanol. (b) McKee, V.; Zvagulis, M.; Dagdigian, J. V.; Patch, M. G.; Reed, C. A. *J. Am. Chem. Soc.* **1984**, *106*, 4765.

(11) (a) Satcher, J. H., Jr.; Droege, M. W.; Weakley, T. J. R.; Taylor, R. T. *Inorg. Chem.* **1995**, *34*, 3317. (b) Droege, M. W.; Satcher, J. H., Jr.; Reibold, R. A.; Weakely, T. J. R. *Prepr. Pap.*−*Am. Chem. Soc., Div. Fuel Chem.* **1992**, *37* (1), 340.

(12) Satcher, J. H., Jr.; Balch, A. L.; Olmstead, M. M.; Droege, M. W. *Inorg. Chem.* **1996**, *35*, 1749.

(13) Euerling, B.; Schmidt, M.; Pinkernell, U.; Karst, U.; Krebs, B. *Angew. Chem., Int. Ed. Engl.* **1996**, *35*, 1973.

Table 1. Selected Bond Lengths and Angles for $[Fe_4(\mu\text{-}O)_2(\mu\text{-}BMDP)_2(\mu\text{-}OAc)_2](NO_3)_3(OH)\cdot 12H_2O$[a]

Bond Lengths (Å)			
Fe(1)−O(1)	1.772(5)	Fe(1)−O(2)	1.978(5)
Fe(1)−O(4)	1.958(5)	Fe(1)−N(1)	2.201(6)
Fe(1)−N(4)	2.074(6)	Fe(2)−O(1)	1.810(5)
Fe(2)−O(3)	2.085(5)	Fe(2)−O(4)	2.026(5)
Fe(2)−N(2)	2.322(6)	Fe(2)−N(6)	2.089(6)
Fe(2)−N(8)	2.101(7)		

Bond Angles (deg)			
Fe(1)−O(1)−Fe(2)	128.4(3)	Fe(1)−O(4)−Fe(2)	124.9(2)
O(1)−Fe(1)−O(4)	113.9(2)	O(1)−Fe(1)−O(2)	104.1(2)
O(4)−Fe(1)−O(2)	90.9(2)	O(1)−Fe(1)−N(4)	112.4(2)
O(4)−Fe(1)−N(4)	131.4(2)	O(2)−Fe(1)−N(4)	91.6(2)
O(1)−Fe(1)−N(1)	103.8(2)	O(4)−Fe(1)−N(1)	77.8(2)
O(2)−Fe(1)−N(1)	152.1(2)	N(4)−Fe(1)−N(1)	77.8(2)
O(1)−Fe(2)−O(4′)	106.9(2)	O(1)−Fe(2)−O(3)	96.4(2)
O(4′)−Fe(2)−O(3)	84.4(2)	O(1)−Fe(2)−N(6′)	106.0(2)
O(4′)−Fe(2)−N(6′)	88.4(2)	O(3)−Fe(2)−N(6′)	157.6(2)
O(1)−Fe(2)−N(8′)	100.3(2)	O(4′)−Fe(2)−N(8′)	152.3(2)
O(3)−Fe(2)−N(8′)	87.5(2)	N(6′)−Fe(2)−N(8′)	89.0(2)
O(1)−Fe(2)−N(2′)	172.7(2)	O(4′)−Fe(2)−N(2′)	79.4(2)
O(3)−Fe(2)−N(2′)	80.3(2)	N(6′)−Fe(2)−N(2′)	77.5(2)
N(8′)−Fe(2)−N(2′)	73.1(2)		

[a] Symmetry transformations used to generate equivalent atoms: (′) $-x, -y + 1, -z + 1$.

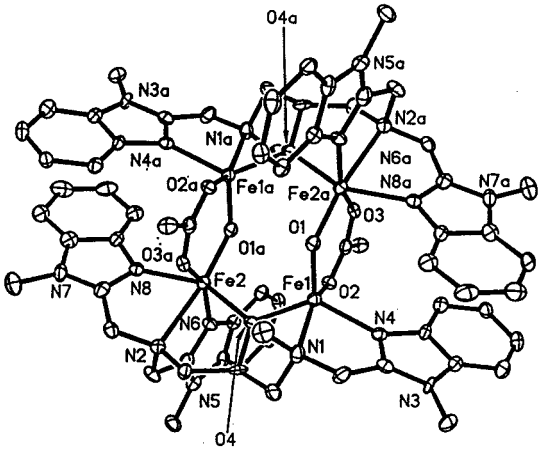

Figure 1. Perspective view of the tetranuclear cation, $[Fe_4(\mu\text{-}O)_2(\mu\text{-}BMDP)_2(\mu\text{-}OAc)_2]^{4+}$, with partial atom labels and numbering scheme. Hydrogen atoms were omitted for clarity. Thermal contours are shown at the 30% level.

(e.g., tetrafluoroborate, tetraphenylborate) did not yield homogeneous, crystalline products. Attempts to recrystallize $[Fe_4(\mu\text{-}O)_2(\mu\text{-}BMDP)_2(\mu\text{-}OAc)_2](NO_3)_3(OH)\cdot 6H_2O$ were unsuccessful due to the insolubility of the nitrate salt in common solvents and in water.

Efforts to increase the solubility of $[Fe_4(\mu\text{-}O)_2(\mu\text{-}BMDP)_2(\mu\text{-}OAc)_2](NO_3)_3(OH)\cdot 6H_2O$ by metathesis with sodium tetrafluoroborate resulted in the isolation of crystals of a new octanuclear iron species, $[Fe_8(\mu\text{-}O)_4(\mu\text{-}BMDP)_4(OH)_4(\mu\text{-}OAc)_4](BF_4)_3(OH)\cdot 2CH_3CN\cdot 8H_2O$ ($[\mathbf{2}](BF_4)_3(OH)\cdot 2CH_3CN\cdot 8H_2O$).

Crystal and Molecular Structure of $[Fe_4(\mu\text{-}O)_2(\mu\text{-}BMDP)_2(\mu\text{-}OAc)_2](NO_3)_3(OH)\cdot 12H_2O$. Selected interatomic distances and angles are given in Table 1. A view of the tetracation $[\mathbf{1}]^{4+}$ is shown in Figure 1, while structural details of the central core unit are more clearly revealed in Figure 2, where only the first coordination sphere about each iron center is shown. The complex consists of four iron(III) ions, two (μ-BMDP) ligands, two doubly bridging oxide ions, and two bridging acetate groups. Additionally, there are four counterions in two crystallographic sites. One of these sites is disordered and occupied equally by

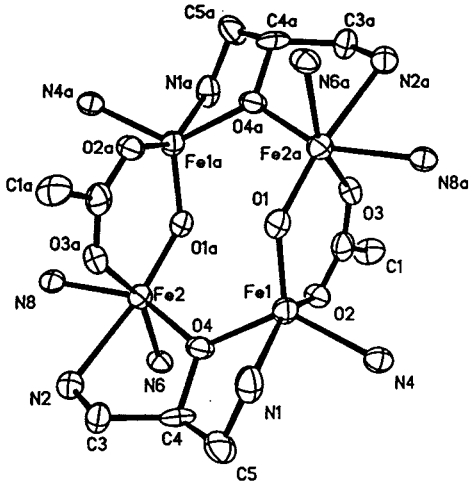

Figure 2. Inner coordination sphere of $[Fe_4(\mu\text{-}O)_2(\mu\text{-}BMDP)_2(\mu\text{-}OAc)_2]^{4+}$. The thermal contours are shown at the 30% level.

a nitrate ion and a hydroxide ion. None of these counterions are involved in iron coordination. Also there is a considerable amount of water in the crystals used for the structure determination which were not subjected to vacuum-drying. Each binucleating (μ-BMDP) ligand coordinates to two iron(III) ions and causes these two ions to become structurally distinct. The two iron ions bound to one (μ-BMDP) ligand are also linked to the iron ions of a second, identical binuclear unit by external bridging oxide and acetate groups. Within the binuclear unit, Fe(1) is five-coordinate with distorted square pyramidal geometry and a N_2O_3 donor set. The (μ-BMDP) ligand coordinates to Fe(1) through an amine, benzimidazole, and bridging alkoxide groups. The coordination sphere of Fe(1) is completed by the external bridging oxide ion, O(1), and a bridging carboxylate ion, O(2). Fe(2) is six-coordinate with distorted octahedral geometry and an N_3O_3 donor set. The (μ-BMDP) ligand coordinates to Fe(2) via an amine, two benzimidazoles, and the bridging alkoxide groups. An external bridging oxide ion, O(1A), and an acetate ion, O(3A), complete the coordination sphere about Fe(2).

The pair of iron atoms that are connected by the (μ-BMDP) ligand are joined through the oxo and carboxylato bridges to form the tetranuclear core. That core is constructed about a center of symmetry, and the four-iron unit is planar. The Fe···Fe separations are 3.532(4) and 3.224(4) Å across the alkoxo and oxo bridges, respectively. The Fe−O oxo bond lengths are 1.772(5) and 1.810(5) Å for the five-coordinate and six-coordinate iron centers, respectively. These bond lengths span the range (1.76−1.82 Å) that is reported for iron oxo bonds.[14] In general, for μ-oxo monobridged complexes, shorter bond lengths are found in compounds with lower coordination number.[8b] The Fe−O−Fe angle of 128.4(3)° lies at the low end of the range (116−180°) found for a variety of oxo-bridged complexes.[8b,14] Similar angles in other $Fe_2(\mu\text{-}O)(\mu\text{-}O_2R)$ units include 128.3° in $[Fe_2(\mu\text{-}O)(\mu\text{-}OBz)(hdp)_2]BPh_4$, 129.7° in $[Fe_2(\mu\text{-}O)(\mu\text{-}OBz)(tpa)_2](ClO_4)_3$, and 129.2° in $[Fe_2(\mu\text{-}O)(\mu\text{-}OAc)(tpa)_2](ClO_4)_3\cdot 2H_2O$.[8b] The Fe−O (alkoxo) bond lengths are 1.958(5) and 2.026(5) Å for the five-coordinate and six-coordinate iron centers, respectively. The Fe−O(R)−Fe angle in this unit is 124.9(2)°.

A comparison of selected bond lengths and angles for $[\mathbf{1}]^{4+}$ and the related tetranuclear complexes, $[Fe_4(\mu\text{-}O)_2(\mu\text{-}TBDP)_2(\mu\text{-}OAc)_2]^{4+}$ and $[Fe_4(\mu\text{-}O)_2(\mu\text{-}HPTA)_2(\mu\text{-}CO_3)_2]$,[6−16] are given

(14) Murray, K. S.; *Coord. Chem. Rev.* **1974**, *12*, 1.

Table 2. Comparison of Structural Data for Tetranuclear Iron(III) Complexes

parameter	$[Fe_4(\mu\text{-}O)_2(\mu\text{-}BMDP)_2(\mu\text{-}OAc)_2]^{4+}$	$[Fe_4(\mu\text{-}O)_2(HPTA)_2(\mu\text{-}CO_3)_2]^{6-}$ [a]	$[Fe_4(\mu\text{-}O)_2(\mu\text{-}TBDP)_2(\mu\text{-}OAc)_2]^{4+}$ [b]
Fe−O(oxo), Å	1.772(5), 1.810(5)	1.829(4)	1.796(9)
Fe−O(alkoxo), Å	1.958(5), 2.026(5)	2.05(1)	2.023(8)
Fe−O(OAc), Å	1.978(5), 2.085(5)	1.992(4)	2.010[c]
Fe−O(oxo)−Fe, deg	128.4(3)	136.4(3)	172.6(1)
Fe−O(alkoxo)−Fe, deg	124.9(2)	132.3(2)	120.9(4)
Fe(1)···Fe(2) (oxo), Å	3.224(4)	3.397	3.586(3)
Fe(1)···Fe(2) (alkoxo), Å	3.532(4)	3.755	3.488(2)

[a] Reference 16. [b] Reference 15. [c] Average value.

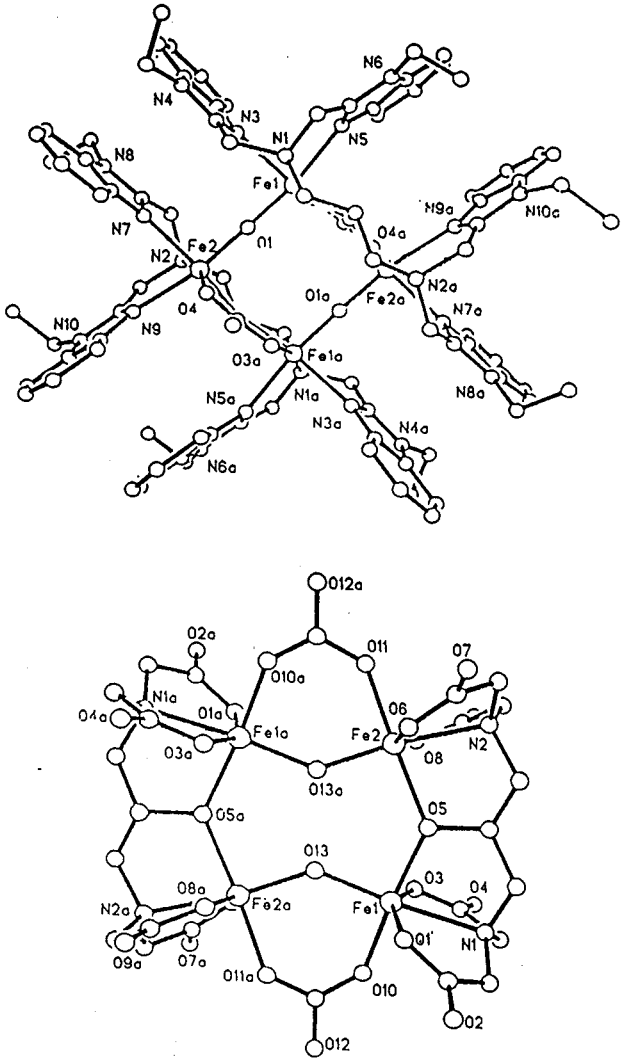

Figure 3. Views of two related tetranuclear cations, $[Fe_4(\mu\text{-}O)_2(\mu\text{-}TBDP)_2(\mu\text{-}OAc)_2]^{4+}$ (from data in ref 15) and $[Fe_4(\mu\text{-}O)_2(\mu\text{-}HPTA)_2(\mu\text{-}CO_3)_2]^{6-}$ (from data in ref 16).

in Table 2, while Figure 3 shows the three-dimensional structures of these two complexes. These cationic complexes also consist of two bridging, binucleating ligands and four iron ions, as well as two bridging carboxylate (or carbonate) ligands and two oxo bridges. In $[Fe_4(\mu\text{-}O)_2(\mu\text{-}HPTA)_2(\mu\text{-}CO_3)_2]^{6-}$ an alkoxo bridge is formed between the two iron ions that are connected by one (μ-HPTA) ligand. Dimerization of this binuclear unit occurs through an oxo and a carbonatato bridge in a fashion similar to that found in $[\mathbf{1}]^{4+}$. For $[Fe_4(\mu\text{-}O)_2(\mu\text{-}TBDP)_2(\mu\text{-}OAc)_2]^{4+}$, alkoxo and acetato bridges are formed between the iron centers that are connected by a single binucleating (μ-TBDP) ligand, while unsupported μ-oxo linkages complete the tetranuclear structure. Thus, the comparable bridging arrangements in $[\mathbf{1}]^{4+}$ and $[Fe_4(\mu\text{-}O)_2(\mu\text{-}HPTA)_2(\mu\text{-}CO_3)_2]^{6-}$ account for the similarity of iron−oxo angles. On the other hand, stacking of the benzimidazole groups through $\pi-\pi$ interactions from linked binuclear units occurs for $[\mathbf{1}]^{4+}$ in a fashion similar to that found in $[Fe_4(\mu\text{-}O)_2(\mu\text{-}TBDP)_2(\mu\text{-}OAc)_2]^{4+}$. The phenyl rings of two of the three benzimidazole moieties of each binuclear unit in $[\mathbf{1}]^{4+}$ lie parallel to their counterparts, and a plane located between two opposing rings is perpendicular to the plane of the six-membered rings formed by $Fe-O_{oxo}-Fe$ and the carbon and two oxygen atoms of the acetate anion. These latter two rings are themselves parallel but are oriented in an opposite fashion through the inversion center.

Table 3. Mössbauer Parameters of Vacuum-Dried $[Fe_4(\mu\text{-}O)_2(\mu\text{-}BMDP)_2(\mu\text{-}OAc)_2](NO_3)_3(OH)\cdot 6H_2O$

temp	site	ΔE_Q	δ	A_1/A_2[b]
80 K	1	1.40(1)	0.48(1)	0.52
	2	1.20(2)	0.24(1)	
298 K[c]	1	1.29(2)	0.30(1)	0.42
	2	1.14(2)	0.34(1)	

[a] All values are in mm/s relativew to Fe. Number in parentheses is error in last figure. [b] Area of site 1 to area of site 2. [c] Average of two separate spectra.

Mössbauer Spectral Data for $[Fe_4(\mu\text{-}O)_2(\mu\text{-}BMDP)_2(\mu\text{-}OAc)_2](NO_3)_3(OH)\cdot 6H_2O$. The zero-field Mössbauer spectrum of $[Fe_4(\mu\text{-}O)_2(\mu\text{-}BMDP)_2(\mu\text{-}OAc)_2](NO_3)_3(OH)\cdot 6H_2O$ measured at 80 K contains a broad, asymmetric doublet that could be fit to a two-site model with $\delta_1 = 0.48(1)$ mm s^{-1}, $\Delta E_{Q1} = 1.40(1)$ mm s^{-1} and $\delta_2 = 0.24(1)$ mm s^{-1}, $\Delta E_{Q2} = 1.20(2)$ mm s^{-1}. The Mössbauer spectra of both sites indicate that all the iron atoms are in the $S = 5/2$ spin state (Table 3). Generally the more unsymmetrical the environment around the iron, the greater the magnitude of the quadrupole splitting.[17] The five-coordinate iron is in a less symmetrical environment (N_2O_3) relative to the six-coordinate iron (N_3O_3); thus we ascribe the slightly larger quadrupolar splitting found in site 1 to the pentacoordinate irons. Measurement at 298 K using the same model gave $\delta_1 = 0.30(1)$ mm s^{-1}, $\Delta E_{Q1} = 1.29(2)$ mm s^{-1} and $\delta_2 = 0.34(1)$ mm s^{-1}, $\Delta E_{Q2} = 1.14(2)$ mm s^{-1}. Since the donor types are identical, the relatively small difference in quadrupole splitting between the two iron centers may be a consequence of the short iron−oxo bond which dominates the electric field gradient at each metal. In this complex the isomer shift appears to be a more useful indicator for assignment. As the electron density at the iron nucleus decreases, δ increases. For similar donor atoms, average bond lengths are 0.04(1) Å shorter for the five-coordinate iron center than for the six-coordinate iron center. This shortening is a consequence of a reduction of electron

(15) Chen, Q.; Lynch, J. B.; Gomez-Romero, P.; Ben-Hussein, A.; Jameson, G. B.; O'Connor, C. J.; Que, L., Jr. *Inorg. Chem.* **1988**, *27*, 2673.
(16) Jameson, D. L.; Xie, C.-L.; Hendrickson, D. N.; Potenza, J. A.; Schugar, H. J. *J. Am. Chem. Soc.* **1987**, *109*, 740.
(17) Parish, R. V. *NMR, NQR, EPR, and Mössbauer Spectroscopy in Inorganic Chemistry*; Elliss-Horwood: New York, 1990; Chapter 4.

density for the five-coordinate iron. This feature is consistent with the observed isomer shifts at 298 K and leads to the same assignment as predicted by quadrupole splitting.

The spectral areas of each site are proportional to the Mossbauer effect (f), which is defined as $ke^{-\langle x^2\rangle}$, where $\langle x^2\rangle$ is the mean square vibrational amplitude of the absorbing iron nucleus.[18] The $\langle x^2\rangle$ for the six-coordinate iron nucleus would be less than the $\langle x^2\rangle$ in the five-coordinate iron nucleus because the six-coordinate iron ion is in a more restricted environment (N_3O_3) than the five-coordinate iron nucleus (N_2O_3). Thus, the absorption area of the five-coordinate iron would be less than the area of the six-coordinate iron. Because the ratio A_1/A_2 is about 0.4 at room temperature (Table 3), site 1 contains the five-coordinate iron and site 2 the six-coordinate iron, in agreement with the assignments made from the quadrupole splitting and isomer shift values. The difference in the area ratios at the two temperatures indicates that the f factor of the two types of iron varies differently with temperature.

In oxyhemerythrin, purple acid phosphatase, metribonucleotide reductase, and some forms of methane monooxygenase, a pair of quadrupole doublets are seen with isomer shifts in the range 0.44−0.55 mm/s and quadrupole splittings spread over a range 0.87−2.45 mm/s.[4b,g] In each of these proteins, mono- or dicarboxylato-bridged diiron centers are additionally supported by oxo or hydroxo bridges. In the case of $[Fe_4(\mu\text{-}O)_2(\mu\text{-BMDP})_2(\mu\text{-OAc})_2](NO_3)_3(OH)\cdot 6H_2O$, however, both an oxo and alkoxo bridge are found on each iron. This bridging arrangement may be responsible for producing quadrupole splitting values that lie close to the middle of the range reported for the diiron proteins.

Magnetic Susceptibility Results for $[Fe_4(\mu\text{-}O)_2(\mu\text{-BMDP})_2(\mu\text{-OAc})_2](NO_3)_3(OH)\cdot 6H_2O$. Solid-state magnetic susceptibility measurements indicate the presence of strong antiferromagnetic coupling with a room-temperature μ_{eff} value of 1.9 μ_B/Fe. The temperature dependence of the data was evaluated using the Heisenberg−Dirac−van Vleck spin Hamiltonian ($H = -2JS_1S_2$) with an $S_1 = S_2 = 5/2$ basis set. Improved fits were obtained by correcting for the underlying temperature-independent paramagnetism of the Fe(III) ions, including a variable monomeric impurity level, and using the molecular field approximation to determine the value of the cross coupling constant, zJ'.[19] The molar susceptibility is given as

$$\chi_M = (1 - w)(P/Q)2Ng^2\beta^2/k(T - \theta) + \text{tip} + (w)\chi_{para}$$

where $\theta = zJ'(P/Q)$, $P = 2e^A + 10e^B + 28e^C + 60e^D + 110e^E$, $Q = 1 + 3e^A + 5e^B + 7e^C + 9e^D + 11e^E$, $A = 2J/kT$, $B = 6J/kT$, $C = 12J/kT$, $D = 20J/kT$, $E = 30J/kT$, tip = temperature-independent paramagnetism, and $\chi_{para} = (S)(S + 1)(Ng^2\beta^2/3kT)$. This last term accounts for the spin-only magnetism associated with a paramagnetic impurity of spin S at a variable level (w). Although the temperature dependence is difficult to model, a reasonable fit was obtained as shown in Figure 4 for the 6−300K data with $g = 2.0$ (fixed), yielding the following parameters: $J = -103.3$ cm^{-1}, $zJ' = -105.9$ cm^{-1}, tip $= 5.8 \times 10^{-4}$ emu/mol, and an impurity level $w = 0.3\%$ ($R = 0.9980$). Since the molecular field approximation is only valid for $|zJ'| \ll |J|$ (i.e., on the order of 10% of J or less), these values are given only for comparison. These values are consistent with those reported for $[Fe_4(\mu\text{-}O)_2(\mu\text{-HPTA})_2(\mu\text{-}CO_3)_2]^{6-}$ ($\mu_{eff} = 2.4$ μ_B/Fe, $J = -63.4$ cm^{-1}, $J' = -11.2$ cm^{-1})[15] and $[Fe_4(\mu\text{-}O)_2(\mu\text{-TBDP})_2(\mu\text{-OAc})_2]^{4+}$ ($\mu_{eff} = 1.7$ μ_B/Fe, $J = -83$ cm^{-1}, $zJ' = -107$ cm^{-1}).[16] The increase in the calculated values of both the primary and the cross coupling for **1** may be due to a lowering of the effective core symmetry from C_{2h} for $[Fe_4O_2(HPTA)_2(CO_3)_2]^{6-}$ and $[Fe_4(O)_2(TBDP)_2(OBz)_2]^{4+}$ to C_i for $[Fe_4(\mu\text{-}O)_2(\mu\text{-BMDP})_2(\mu\text{-OAc})_2]^{4+}$, which facilitates more symmetry-allowed overlap of metal d orbitals with the alkoxy, acetate, and oxo p orbitals. This observation is in agreement with the effect noted by Jameson in which oxo-bridged, binuclear iron complexes with C_s symmetry were found to exhibit increased antiferromagnetic behavior when compared to their C_{2v} analogues.[20]

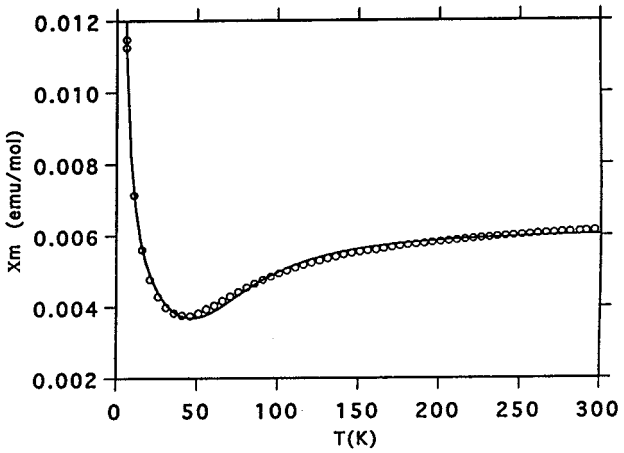

Figure 4. Temperature dependence (6−300 K) of the corrected molar susceptibility for $[Fe_4(\mu\text{-}O)_2(\mu\text{-BMDP})_2(\mu\text{-OAc})_2](NO_3)_3(OH)\cdot 6H_2O$ The solid line is a least-squares fit for all data using the Heisenberg−Dirac−van Vleck spin Hamiltonian with an $S_1 = S_2 = 5/2$ basis set ($H = -2JS_1S_2$) and the molecular field approximation to determine the cross coupling value. Final parameter set for fit with $g = 2.00$ (fixed): $J = -103.3$ cm^{-1}, $zJ' = -105.9$ cm^{-1}, tip $= 5.8 \times 10^{-4}$ emu/mol, and an impurity level $w = 0.3\%$ ($R = 0.9980$).

Crystal and Molecular Structure of $[Fe_8(\mu\text{-}O)_4(\mu\text{-BMDP})_4(OH)_4(\mu\text{-OAc})_4](BF_4)_3(OH)\cdot 2CH_3CN\cdot 8H_2O$. A view of the cation $[Fe_8(\mu\text{-}O)_4(\mu\text{-BMDP})_4(OH)_4(\mu\text{-OAc})_4]^{4+}$, which has crystallographically imposed $\bar{4}$ (S_4) symmetry, is shown in Figure 5 (top), while the structural details of the central core are more clearly revealed in the lower part of that figure. Figure 6 shows the details of the structure at one corner of the nearly square cation. Selected bond lengths and angles for the cation are given in Table 4. The cation is made up of eight iron atoms, four bridging oxide ions, four μ-BMDP ligands, and four bridging acetate ions. In contrast to the arrangement found in **1**, the acetate anions now bridge the two irons that are linked by the alkoxide group to form the binuclear subunit. These four binuclear subunits are linked together by unsupported, nearly linear (Fe−O−Fe angle, 178.0(4)°), oxo bridges. When the cation is viewed perpendicular to the mean plane of the eight iron ions, as is the case in the upper part of Figure 5, four of the iron ions are seen to lie at the corners of a square. The Fe···Fe distance along the edge of the square is 7.4 Å. The other four iron ions lie near the midpoints of the same square. The four hydroxy ligands protrude into the center of this square. Within this group, the adjacent O(5)···O(5A) separation is 2.621 Å, while the trans O(5)···O(5C) distance is 3.697 Å. The separation between adjacent hydroxy groups suggests that there

(18) Debrunner, P. G.; Frauenfelder, H. In *An Introduction to Mössbauer Spectroscopy*; May, L., Ed.; Plenum Press: New York, 1971; pp 16−22.

(19) O'Conner, C. J. *Prog. Inorg. Chem.* **1982**, *29*, 203−283.

(20) Gomez-Romero, P.; Witten, E. H.; Reiff, W. M.; Jameson, G. B. *Inorg. Chem.* **1990**, *29*, 5211. Gomez-Romero, P.; Witten, E. H.; Reiff, W. M.; Backes, G.; Sanders-Loehr, J.; Jameson, G. B. *J. Am. Chem. Soc.* **1989**, *111*, 9039.

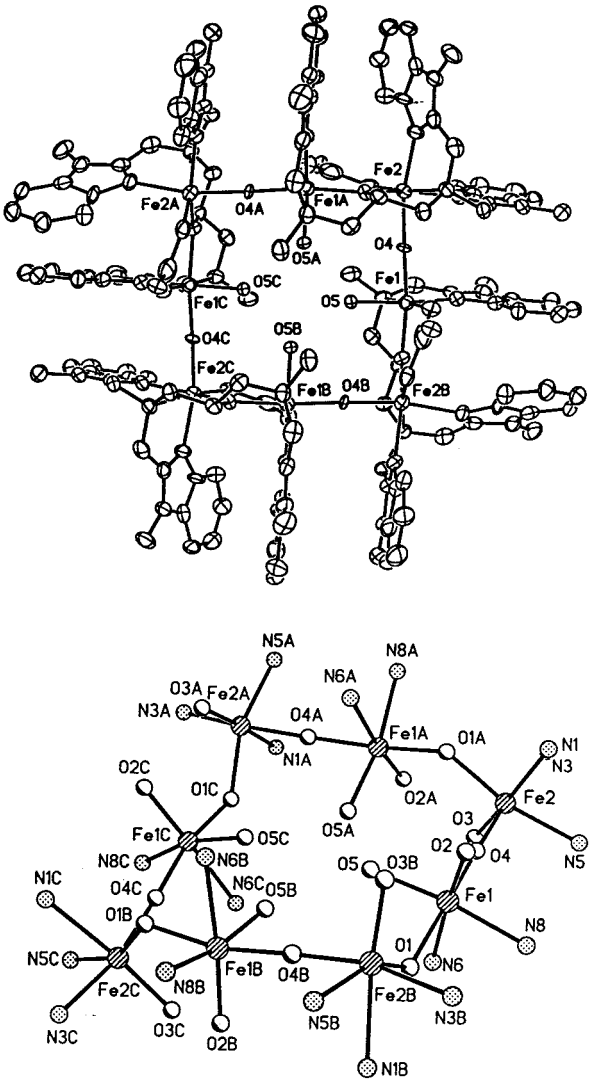

Figure 5. (Top) Structure of the octanuclear Fe(III) cation, $[Fe_8(\mu\text{-}O)_4(\mu\text{-BMDP})_4(OH)_4(\mu\text{-OAc})_4]^{4+}$, with partial atom labels and numbering scheme. Hydrogen atoms were omitted for clarity. The thermal contours are shown at the 30% level. (Bottom) Inner core of the octanuclear cation, $[Fe_8(\mu\text{-}O)_4(\mu\text{-BMDP})_4(OH)_4(\mu\text{-OAc})_4]^{4+}$, with uniform, arbitrarily sized circles for the atoms.

is hydrogen bonding between them. The ability to accommodate a cyclic set of four hydroxy groups connected through hydrogen bonding may play a crucial role in the organization of this complex cation during its formation.

Each (μ-BMDP) ligand is bound to two iron(III) ions. The iron ions are also linked to the iron ions of a second identical binuclear unit by an external bridging oxide group. Within the binuclear unit built about one (μ-BMDP) unit, Fe(1) is six-coordinate with distorted octahedral geometry and an N_2O_4 donor set. The (μ-BMDP) ligand coordinates to Fe(1) with an amine, N(6), benzimidazole, N(8), and bridging alkoxide, O(1), groups. The coordination sphere of Fe(1) is completed by the external bridging oxide ion, O(4), a bridging, bidentate carboxylate ion, O(2), and a terminal hydroxide ion, O(5). Fe(2) is also six-coordinate with distorted octahedral geometry and an N_3O_3 donor set. The (μ-BMDP) ligand bonds to Fe(2) via an amine, N(1), two benzimidazoles, N(3) and N(5), and the bridging alkoxide, O(1), groups. An external bridging oxide ion, O(4), and an acetate ion, O(3), complete the coordination sphere about Fe(2).

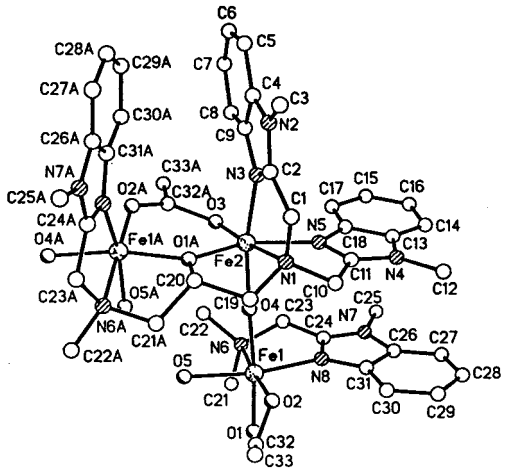

Figure 6. View of one corner of the structure of the octanuclear cation, $[Fe_8(\mu\text{-}O)_4(\mu\text{-BMDP})_4(OH)_4(\mu\text{-OAc})_4]^{4+}$. Atoms are represented by uniform, arbitrarily sized circles. O(1) and O(4A) are bridging oxide ions, while O(5) and O(5A) are hydroxide ligands.

Table 4. Selected Bond Lengths and Angles for $[Fe_8(\mu\text{-}O)_4(\mu\text{-BMDP})_4(OH)_4(\mu\text{-OAc})_4](BF_4)_3(OH)\cdot 2CH_3CN\cdot 8H_2O$[a]

Distances (Å)			
Fe(1)···Fe2(alkoxo)	3.531(7)	Fe(1)···Fe(2a)(oxo)	3.918(8)
Fe(1)−O(1)(alkoxo)	1.992(8)	Fe(1)−O(2)(acetate)	1.870(9)
Fe(1)−O(4)(oxo)	1.947(7)	Fe(1)−O(5)(hydroxide)	1.991(7)
Fe(1)−N(6)(amine)	2.268(11)	Fe(1)−N(8)(benz.)	2.082(11)
Fe(2)−O(1)(alkoxo)	1.984(8)	Fe(2)−O(3)(acetate)	1.836(9)
Fe(2)−O(4)(oxo)	1.971(7)	Fe(2)−N(1)(amine)	2.286(11)
Fe(2)−N(3)(benz.)	2.075(10)	Fe(2)−N(5)(benz.)	2.080(11)
Angles (deg)			
Fe(1)−O(1)−Fe(2)	125.3(4)	Fe(1)−O(4)−Fe(2)	178.0(4)
O(2)−Fe(1)−O(4)	96.1(4)	O(2)−Fe(1)−O(5)	97.6(4)
O(4)−Fe(1)−O(5)	85.9(3)	O(2)−Fe(1)−O(1)	97.0(4)
O(4)−Fe(1)−O(1)	166.8(3)	O(5)−Fe(1)−O(1)	90.9(3)
O(2)−Fe(1)−N(8)	97.4(4)	O(4)−Fe(1)−N(8)	89.4(4)
O(5)−Fe(1)−N(8)	164.7(4)	O(1)−Fe(1)−N(8)	90.3(4)
O(2)−Fe(1)−N(6)	174.9(4)	O(4)−Fe(1)−N(6)	86.1(3)
O(5)−Fe(1)−N(6)	87.1(4)	O(1)−Fe(1)−N(6)	81.0(4)
N(8)−Fe(1)−N(6)	78.0(4)	O(3)−Fe(2)−O(4)	97.6(3)
O(3)−Fe(2)−O(1′)	100.1(4)	O(4)−Fe(2)−O(1′)	88.0(3)
O(3)−Fe(2)−N(3)	95.0(4)	O(4)−Fe(2)−N(3)	166.4(4)
O(1′)−Fe(2)−N(3)	94.5(4)	O(3)−Fe(2)−N(5)	106.1(5)
O(4)−Fe(2)−N(5)	84.0(4)	O(1′)−Fe(2)−N(5)	153.3(4)
N(3)−Fe(2)−N(5)	87.9(4)	O(3)−Fe(2)−N(1)	173.0(4)
O(4)−Fe(2)−N(1)	89.2(3)	O(1′)−Fe(2)−N(1)	78.2(4)
N(3)−Fe(2)−N(1)	78.4(4)	N(5)−Fe(2)−N(1)	76.3(4)

[a] Symmetry transformations used to generate equivalent atoms: (′) $-y + 3/4$, $x - 1/4$, $-z + 3/4$.

The benzimidazole ligands make nearly parallel, face-to-face contact along the outer edges of the square cation.

Discussion

Novel tetranuclear and octanuclear iron(III) complexes have been prepared that exhibit a planar arrangement of the metal centers and form square structural units. The construction of molecular and ionic units according to particular geometric blueprints has become a focus of supramolecular chemistry in recent years.[21,22] This has given rise to the planned synthesis of molecular squares and hexagons as well as other units. In the case of the two iron complexes described here, the iron ions function as corners of the square and the ~90° bond angles that accompany approximate octahedral coordination are clearly appropriate for producing ionic squares of this sort.

(21) Stang, P. J.; Olenyuk, B. *Acc. Chem. Res*. **1997**, *30*, 502.
(22) Bunz, U. H. F. *Angew. Chem., Int. Ed. Engl.* **1994**, *33*, 1073.

While ligands such as HBMDP and HTBDP are well suited for the formation of binuclear complexes, the present study as well as others demonstrates that larger polynuclear units can also form from these ligands when other bridging ligands like oxide or hydroxide are present during the assembly process. Thus, the HBMDP ligand does not contain structural units that inhibit additional bridging as seen here, but the inclusion of such a structural element would give ligands with distinct advantages for controlled synthesis of strictly binuclear species. Iron(III) clusters with as many as 18 and 19 iron ions have been prepared and characterized,[23,24] and a limited number of octanuclear iron systems have been reported.[25−27] None of these complexes have the square geometry that is seen in $[Fe_8(\mu\text{-}O)_4(\mu\text{-BMDP})_4(OH)_4(\mu\text{-OAc})_4]^{4+}$.

Distinct coordination asymmetry is induced on the individual iron sites within $[Fe_4(\mu\text{-}O)_2(\mu\text{-BMDP})_2(\mu\text{-OAc})_2]^{4+}$ and $[Fe_8(\mu\text{-}O)_4(\mu\text{-BMDP})_4(OH)_4(\mu\text{-OAc})_4]^{4+}$ by the presence of the unsymmetrical ligand, HBMDP. In the tetramer, the asymmetry in the ligand induces coordination number asymmetry at the metal sites so that one iron site is five-coordinate while the other is six-coordinate. Mössbauer spectral measurements also indicate the presence of distinguishable iron(III) sites, a feature noted for the non-heme proteins: oxyhemerythrin, methane monooxygenase, ribonucleotide reductase, and purple acid phosphatase. In addition, magnetic measurements indicate the presence of strong antiferromagnetic coupling of the iron centers. This coupling is similar to that found in hemerythrin and purple acid phosphatase and may be, in part, a result of the asymmetry of the complex. Clearly, coordination number asymmetry does not drastically alter the measured properties so that they would lie outside the normal range found for symmetric iron compounds with similar core features. Since these properties are among those used to deduce coordination environments in metalloproteins, it is important to utilize a variety of well-defined models to interpret these spectroscopic measurements with confidence.

Metathesis of $[Fe_4(\mu\text{-}O)_2(\mu\text{-BMDP})_2(\mu\text{-OAc})_2](NO_3)_3(OH)\cdot 6H_2O$ with sodium tetrafluoroborate resulted in the isolation of crystals of the octanuclear iron species, $[Fe_8(\mu\text{-}O)_4(\mu\text{-BMDP})_4(OH)_4(\mu\text{-OAc})_4](BF_4)_3(OH)\cdot 2CH_3CN\cdot 8H_2O$ (**2**). The cation present in this salt also has a square structure with iron ions again providing the angular arrangement necessary for the construction of the corners in the ion. This ion with its larger size has a more open core that has accommodated the bonding of hydroxide ions onto Fe(2). These hydroxide ions protrude into the center of the square. The more congested structure of $[Fe_4(\mu\text{-}O)_2(\mu\text{-BMDP})_2(\mu\text{-OAc})_2]^{4+}$ lacks this feature, and it is likely that steric congestion is, in part, responsible for the presence of the five-coordinate iron sites within this tetranuclear cation.

Experimental Section

Materials. Acetone (Aldrich), sodium acetate trihydrate (Aldrich), and iron(III) nitrate nonahydrate (Alfa) were purchased and used without purification. *N,N,N′*-Tris((*N*-methyl)-2-benzimidazolylmethyl)-*N′*-methyl-1,3-diamino-2-propanol [HBMDP] was prepared as previously described.[11]

(23) Watton, S. P.; Fuhrmann, P.; Pence, L. E.; Caneschi, A.; Cornia, A.; Abbati, G. L.; Lippard, S. J. *Angew. Chem., Int. Ed. Engl.* **1997**, *36*, 1774.
(24) Heath, S. L.; Powell, A. K. *Angew. Chem., Int. Ed. Engl.* **1992**, *31*, 191.
(25) Wieghardt, K.; Pohl, K.; Jibril, I.; Huttner, G. *Angew. Chem., Int. Ed. Engl.* **1984**, *23*, 77.
(26) Delfs, C. D.; Gatteschi, D.; Pardi, L.; Sessoli, R.; Wieghardt, K.; Hanke, D. *Inorg. Chem.* **1993**, *32*, 3099.
(27) Dell'Amica, D. B.; Calderazzo, F.; Labella, L.; Maichle-Mossmer, C. Strahle, J. *J. Chem. Soc., Chem. Commun.* **1994**, 1555.

Table 5. Crystallographic Data

	$[Fe_4(\mu\text{-}O)_2(\mu\text{-BMDP})_2(\mu\text{-OAc})_2](NO_3)_3(OH)\cdot 12H_2O$	$[Fe_8(\mu\text{-}O)_4(\mu\text{-BMDP})_4(OH)_4(\mu\text{-OAc})_4](BF_4)_3(OH)\cdot 2CH_3CN\cdot 8H_2O$
molecular formula	$C_{66}H_{89}Fe_4N_{19}O_{30}$	$C_{136}H_{167}B_3F_{12}Fe_8N_{34}O_{29}$
fw	1851.96	3461.36
color	red	brown
a, Å	12.228(3)	38.555(3)
b, Å	13.915(3)	38.555(3)
c, Å	14.120(3)	11.865(2)
α, deg	115.99(2)	90
β, deg	108.02(2)	90
γ, deg	95.73(2)	90
V, Å^3	1974.2(8)	17637(2)
space group	$P\bar{1}$	$I4_1/a$
Z	1	4
ρ_{calc}, g/cm^{-3}	1.558	1.293
λ, Å	1.541 78 (Cu Kα)	1.541 78 (Cu Kα)
μ (mm^{-1})	6.60	5.83
T, K	130(2)	130(2)
R1[a]	0.071	0.118
wR2[b]	0.225	0.384

[a] $R1 = \sum||F_o| - |F_c||/\sum|F_o|$ (observed data, $F_o > 4\sigma(F_o)$). [b] $wR2 = [\sum[w(F_o^2 - F_c^2)^2]^2/\sum[w(F_o^2)^2]]^{1/2}$ (all data)940.

Synthesis. $[Fe_4(\mu\text{-}O)_2(\mu\text{-BMDP})_2(\mu\text{-OAc})_2](NO_3)_3(OH)\cdot 6H_2O$ ([1]$(NO_3)_3(OH)\cdot 6H_2O$). A solution of ferric nitrate nonahydrate (0.728 g, 1.80 mmol) in 3 mL of water was added dropwise to a stirred solution of HBMDP (0.500 g, 0.90 mmol) in 5 mL of acetone to form a dark red-brown solution. Sodium acetate trihydrate (0.368 g, 2.70 mmol) dissolved in 2 mL of water was then added dropwise to produce a dark red solution, which was covered and stirred at room temperature for 1 h. The solution was then allowed to undergo slow evaporation for 4−5 days (approximately 20% total solvent loss), during which time well-formed wine-red crystals deposited. The crystalline mass was collected by filtration on a glass frit, washed with 3 × 3 mL water, and dried under vacuum at 80 °C for 12 h to produce 0.143 g (18.9%) of a light brown polycrystalline powder. Anal. Calcd for $C_{66}H_{89}Fe_4N_{19}O_{24}$: C, 45.14; H, 5.10; N, 15.16; Fe, 12.72 Found: C, 45.02; H, 4.63; N, 15.78; Fe, 13.03.

$[Fe_8(\mu\text{-}O)_4(\mu\text{-BMDP})_4(OH)_4(\mu\text{-OAc})_4](BF_4)_3(OH)\cdot 2CH_3CN\cdot 8H_2O$ (2). Solid $[Fe_4(\mu\text{-}O)_2(\mu\text{-BMDP})_2(\mu\text{-OAc})_2](NO_3)_3(OH)\cdot 6H_2O$ (0.1022 g, 0.059 mmol) was suspended in 20 mL of acetonitrile. Four equivalents of solid sodium tetrafluoroborate (0.028 g, 0.26 mmol) was added to this suspension. The resulting mixture was covered with Parafilm and stirred overnight to produce a dark brown solution with a fine suspended solid. The mixture was filtered on a fine sintered-glass frit, and the filtrate was placed in a beaker and covered with Parafilm. Several 20 gauge needle holes were made in the film to allow for slow evaporation. When the volume had been reduced to ∼3 mL, large brown crystals had deposited on the sides and bottom of the beaker. The clear brown supernatant liquid was decanted, and the crystalline mass was washed with 3 × 3 mL of water and then dried under vacuum at 80 °C for 12 h to yield 0.0275 g (26.1%) of a light brown, polycrystalline powder.

X-ray Crystallography for $[Fe_4(\mu\text{-}O)_2(\mu\text{-BMDP})_2(\mu\text{-OAc})_2](NO_3)_3(OH)\cdot 12H_2O$ ([1]$(NO_3)_3(OH)\cdot 12H_2O$). Crystals of [**1**]$(NO_3)_3(OH)\cdot 12H_2O$ suitable for X-ray structural determination were obtained by slow evaporation from the original reaction solution. A red, prismatic crystal (0.06 mm × 0.10 mm × 0.15 mm) of [**1**]$(NO_3)_3(OH)\cdot 12H_2O$ was coated with an inert hydrocarbon oil (Paratone-n, Exxon) immediately after removal from solution and mounted on a Siemens P4RA rotating anode diffractometer equipped with a locally modified LT-2 low-temperature device. Intensity data were collected using nickel-filtered Cu Kα radiation. A summary of the crystal data is given in Table 5. Two check reflections showed only random (<1%) variation in intensity during data collection. The data were corrected for Lorentz and polarization effects. Further details are given in the Supporting Information.

Solution and Structure Refinement. Calculations were performed with SHELXTL 5 series of programs. Scattering factors and correction

for anomalous dispersion were taken from a standard source.[28] An absorption correction was applied.[29] The solution was determined by direct methods and subsequent cycles of least-squares refinement and calculation of difference Fourier maps. The atoms within the cation, $[\mathbf{1}]^{4+}$, are fully ordered. Hydrogen atoms were included at geometrically appropriate positions and were refined with a riding model except for the methyl hydrogen atoms, which were refined as a rigid group to make the best fit with small peaks observed in a difference Fourier map in the vicinity the methyl carbon atoms. Methyl hydrogen atoms were assigned isotropic thermal parameters equal to 1.5 times those of the bonded carbon atom; all other hydrogen atom thermal parameters were 1.2 times those of the bonded atom. Within the asymmetric unit there are two sites for nitrate ions. One of the nitrate ions is ordered. The other is apparently not present at full occupancy, and for simplicity it was assigned a value of 0.5 occupancy. The geometry of the disordered nitrate was restrained to fit that of the ordered nitrate (SAME routine of SHELXL). Another atom was found at the same site as the disordered nitrate, and this was assumed to be the 0.5 hydroxide that must be present for charge balance. The remaining difference map densities with interatomic vectors corresponding to hydrogen-bonded water molecules were assigned as oxygen atoms with occupancies as follows: O(1W), O(2W), O(5W), 1.0; O(4W), O(6W), O(7W), O(8W), 0.5; O(3W), O(9W), O(10W), O(11W), 0.25. The refined isotropic thermal parameters show that these assignments are reasonable. No hydrogen atoms for these disordered groups were included in the model. Anisotropic thermal parameters were used for all non-hydrogen atoms in the cation and in the ordered nitrate ion. The largest peak in a final difference map was 0.89 e $Å^{-3}$, which is 0.81 Å from O(2W).

X-ray Crystallography for $[Fe_8(\mu\text{-}O)_4(\mu\text{-}BMDP)_4(OH)_4(\mu\text{-}OAc)_4](BF_4)_3(OH)\cdot 2CH_3CN\cdot 8H_2O$ (2). Diffraction quality crystals of $[Fe_8(\mu\text{-}O)_4(\mu\text{-}BMDP)_4(OH)_4(\mu\text{-}OAc)_4](BF_4)_3(OH)\cdot 2CH_3CN\cdot 8H_2O$ were prepared as described above, but were removed directly from the mother liquor, coated with oil, and placed immediately in the cold stream of the diffractometer. Data collection proceeded as described above.

Solution and Structure Refinement. Solution and refinement followed the procedure utilized in the preceding structure. The cation, $[\mathbf{2}]^{4+}$, is ordered. Hydrogen atoms were added as described above for $[\mathbf{1}]^{4+}$. A symmary of crystal data is contained in Table 5. There are two sites of the tetrafluoroborate ions in the asymmetric unit. In a manner similar to that used in the refinement strategy for $[\mathbf{1}]^{4+}$, the parameters for a more ordered tetrafluoroborate ion at one site were used to provide restraints for a less ordered tetrafluoroborate ion at the second site. A hydroxide ion was also located at the site of the second tetrafluoroborate ion. However, all of the atoms at these sites had only partial occupancy. Several water molecules were also located, as well as a molecule of acetonitrile at half occupancy. The assigned occupancies for the atoms in question are {B(1), F(1), F(2), F(3), F(4)} at 0.5 occupancy; {B(2), F(5), F(6), F(7), F(8)} at 0.25 occupancy, this site shared with O(10) at 0.25 occupancy; {O(6), O(9)} at 0.5 occupancy; {O(7), O(8), O(11), O(12)} at 0.25 occupancy; and an acetonitrile molecule, {N(9), C(34), C(35)} at 0.5 occupancy. Anisotropic thermal parameters were used for all non-hydrogen atoms in the cation and in the molecule of acetonitrile. The largest feature in the final difference electron density map is 1.41 e $Å^{-3}$, which is 1.00 Å from F(4). The relatively high R values apparently stem from the degree of disorder present and the lack of high-angle scattering.

Mössbauer Spectral and Magnetic Susceptibility Measurements. The Mössbauer spectra were obtained on vacuum-dried samples mounted in polyethylene cells using a Ranger Scientific MS-900 spectrometer in acceleration mode with moving source geometry at 80 K and room temperature. The resultant spectra were analyzed by a constrained, least-squares fit to Lorentzian-shaped lines.[30] The velocity range was calibrated with sodium nitroprusside, and the isomer shift values were converted to the iron standard by subtracting 0.257 mm/s.

Magnetic susceptibility measurements were obtained at an applied field of 1 kOe on a Quantum Design SQUID magnetometer operating between 6 and 300 K. Measurement of the magnetic moment at 6 K as a function of field between 0.1 and 30 kOe demonstrated the lack of saturation effects. Determinations were made on finely ground vacuum-dried samples loaded into gelatin capsules. Diamagnetic corrections for the capsules were made by direct measurement, while correction for the ligand, HBMDP, was calculated by use of Pascal's constants.[31] Calibration of the instrument was performed using $HgCo(SCN)_4$.[19]

Acknowledgment. We are grateful to the Gas Research Institute (GRI), Department of Energy, Morgantown Energy and Technology Center (DOE-METC), and the Lawrence Livermore National Laboratory, Institutional Research and Development Program (LLNL Directors Initiative), for their generous support. Work was performed under the auspices of the U.S. Department of Energy by the Lawrence Livermore National Laboratory under contract No. W-7405-ENG-48.

Supporting Information Available: Tables of crystal data, atomic coordinates and equivalent isotropic displacement parameters, bond lengths and angles, anisotropic displacement parameters, and hydrogen coordinates for $[Fe_4(\mu\text{-}O)_2(\mu\text{-}BMDP)_2(\mu\text{-}OAc)_2](NO_3)_3(OH)\cdot 12H_2O$ and $[Fe_8(\mu\text{-}O)_4(\mu\text{-}BMDP)_4(OH)_4(\mu\text{-}OAc)_4](BF_4)_3(OH)\cdot 2CH_3CN\cdot 8H_2O$ (24 pages). X-ray crystallographic files in CIF format for $[Fe_4(\mu\text{-}O)_2(\mu\text{-}BMDP)_2(\mu\text{-}OAc)_2](NO_3)_3(OH)\cdot 12H_2O$ and $[Fe_8(\mu\text{-}O)_4(\mu\text{-}BMDP)_4(OH)_4(\mu\text{-}OAc)_4](BF_4)_3(OH)\cdot 2CH_3CN\cdot 8H_2O$ are available on the Internet only. Access and ordering information is given on any current masthead page.

IC9802404

(28) *International Tables for Crystallography*; Wilson, A. J. C., Ed.; Kluwer Academic Publishers: Dordrecht, 1992; Vol. C.
(29) Parkin, S.; Moezzi, B.; Hope, H. *J. Appl. Crystallogr.* **1995**, *28*, 53.
(30) Stone, A. J. *J. Chem. Soc. A* **1967**, 1971.
(31) Carlin, R. L. *Magnetochemistry*; Springer-Verlag: Berlin, 1986; pp 2−4.